AJNR

Digitized Cerebral Synchrotron Radiation Angiography: Quantitative Evaluation of the Canine Circle of Willis and Its Large and Small Branches

Etsuro Tanaka, Akira Tanaka, Takafumi Sekka, Yoshiro Shinozaki, Kazuyuki Hyodo, Keiji Umetani and Hidezo Mori

AJNR Am J Neuroradiol 1999, 20 (5) 801-806
http://www.ajnr.org/content/20/5/801

AJNR Am J Neuroradiol 20:801–806, May 1999

Digitized Cerebral Synchrotron Radiation Angiography: Quantitative Evaluation of the Canine Circle of Willis and Its Large and Small Branches

Etsuro Tanaka, Akira Tanaka, Takafumi Sekka, Yoshiro Shinozaki, Kazuyuki Hyodo, Keiji Umetani, and Hidezo Mori

BACKGROUND AND PURPOSE: **Conventional X-ray angiography lacks the sensitivity and spatial resolution needed to detect small amounts of iodinated contrast material and to quantitate diameters of the small vessels in the brain. The purpose of this study was to ascertain whether digitized synchrotron radiation microangiography, with the use of a high-definition TV camera system, can accurately show small cerebral vessels.**

METHODS: **Six anesthetized dogs were exposed to monochromatic synchrotron radiation with an energy level of 33.3 keV optimized for iodine detection while iodinated contrast material was injected into the brachiocephalic and vertebral arteries. The images were detected with a high-definition TV camera system with a spatial resolution of 30 μm. In all, 26 cerebral angiograms of the circle of Willis with its branches were obtained, and the images were digitized at a workstation.**

RESULTS: **The small branches of the circle of Willis were clearly visible on all images. Vasodilatation of the circle of Willis and its large and small branches induced by CO_2 inhalation was quantitatively confirmed on the images: for example, the diameter of one small branch was increased from 0.24 ± 0.04 mm to 0.38 ± 0.12 mm. Temporal subtraction improved the image quality.**

CONCLUSION: **The synchrotron radiation angiographic system is useful for visualizing large and small vessels deep in the brain as well as for quantitating their diameters.**

It is known that small-vessel disease in the brain causes lacunar strokes and that some patients with lacunar strokes have a high rate of recurrence (21%) during a 3-year follow-up period (1) and of death (6% to 20%) due to stroke during a 3- to 5-year follow-up period (1–3). Therefore, clinical detection of small-vessel disease would be crucial for predicting a possibility of strokes and for avoiding risk factors for a life-threatening cerebral attack. Unfortunately, conventional imaging data are neither prognostic indicators in patients with lacunar strokes (2, 4) nor useful for evaluating liable small-vessel abnormalities, as conventional X-ray angiography has neither the sensitivity needed to detect small amounts of iodinated contrast material nor the spatial resolution to quantitate the diameters of small vessels in the brain. With the conventional system, small arteries, such as the anterior choroidal artery, cannot always be observed, and quantification of the diameters is not possible in vessels with a diameter of less than 300 μm (5).

Recently, we developed a microangiographic system with high contrast resolution and high spatial resolution, using monochromatic synchrotron radiation as an X-ray source and a high-definition TV camera system as a detector (6). This system allowed depiction of small vessels of the heart (penetrating transmural artery), brain (small branches arising from the circle of Willis), and intestinal organs (vasa recta and their submucosal

Received September 21, 1998; accepted after revision January 9, 1999.

Supported by Grants-in-Aid for Scientific Research (08877118, 09670756, and 10470171) from the Ministry of Education, Science, Sports and Culture of Japan, ''Research for the Future'' Program by the Japan Society for the Promotion of Science (JSPS-RFTF97I00201), Tokai University School of Medicine Project Research and Research Aid, and Eisai Pharmaceutical Co. Ltd. This project was approved as a Joint Research Program of the National Laboratory for High Energy Physics, Tsukuba, Japan (93G241, 95G113, 95G287 and 98G195).

From the Departments of Physiology (E.T., A.T., Y.S., H.M.) and Surgery (T.S.), Tokai University School of Medicine, Isehara, Japan; the National Laboratory for High Energy Physics, Tsukuba, Japan (K.H.); and Synchrotron Radiation Research Institute, Mikazuki, Hyogo Japan (K.U.)

Address reprint requests to Hidezo Mori, MD, Department of Physiology, Tokai University School of Medicine, Isehara 259–1193, Japan.

communications) and of small branches (down to the fifth order) of the pancreatic duct. The aim of this study was to improve this microangiographic system by applying digital processing so as to allow visualization of small vessels deep in the brain and objective measurement of their diameters. The actual diameter changes in large and small vessels around the circle of Willis induced by CO_2 inhalation or partial occlusion of cerebral blood vessels were quantitated semiautomatically.

Methods

Angiographic System

The fundamental design of our synchrotron radiation angiographic system was reported previously (6) (Fig 1A). Briefly, monochromatic synchrotron radiation with an energy level of 33.3 keV was obtained from beamlines NE5 and BL-14 in the National Laboratory for High Energy Physics, Tsukuba, Japan (7, 8). The contrast images of the object together with the reference copper wire with a diameter of 130 μm were formed on a fluorescent screen (HR-mammno, Fuji Film, Tokyo), where a 20 $\times$ 20-mm area was scanned with 15 frames per second for 6 seconds by a high-definition TV camera with 1125 TV lines. This camera is an image pick-up tube with an amorphous selenium photoconductive target and is characterized by its internal amplification process, which uses the avalanche phenomenon in a photoconductive layer (9–11). Electron-hole charge-pairs produced in the amorphous selenium layer are multiplied 32 times by avalanche multiplication to produce the output-signal current (11). The lens-coupling efficiency is also of great importance in attaining a radiographic quantum-noise–limited system, as described in previous articles (6, 11). We set lenses with a small F number (0.65) and a small demagnification factor (1.6:1) between the fluorescent screen and the camera in order to reduce a secondary quantum sink (11). The images were stored as a digital image (1024 $\times$ 1024 pixels, 12 bits per pixel, in a frame memory or a digital audiotape [DAT]). The general system was controlled with a workstation (HP-9000, Hewlett-Packard). The spatial resolution limit of this system was 16 line pairs per millimeter (lp/mm) studied with a modulate-transfer-function chart (MICK type 14: 2.0–20.0 lp/mm, Germany). As for contrast resolution with a vascular phantom (Type 76–700, Nuclear Associates, New York, NY), the minimum size (0.5-mm diameter) vascular phantom with a minimum concentration of contrast material (2.5 mg/mL of iodine) was visible through an acrylic block with a 75-mm thickness. With the current system, the detection limit is 95, 60, and 52 μm for vessels in the canine heart (12), brain (see Results section), and intestinal organs (12), respectively.

Experimental Protocol

All animal experiments were performed in accordance with the Guidelines of Tokai University School of Medicine on Animal Use, which conform to the ''Guide for the Care and Use of Laboratory Animals'' (DHEW publication no. NIH 86–23, revised 1985, Offices of Science and Health Reports, DRR/NIH, Bethesda, MD).

Six beagle dogs (8–11 kg) were used, from which 26 cerebral angiograms were obtained. All six dogs were anesthetized with subcutaneous morphine hydrochloride (3 mg/kg) and intravenous α-chloralose (80 mg/kg) and were intubated and artificially ventilated with air mixed with oxygen at 1 to 3 L/min, a single ventilation volume of 15 to 20 mL/kg, and a respiratory rate of 15 to 20 per minute using a Harvard respirator to maintain PaO_2 at approximately 100 mm Hg, $PaCO_2$ between 25 and 40 mm Hg, and pH between 7.35 and 7.45, as described previously (13). A 7F catheter was placed in the abdominal aorta via the right femoral artery to record the aortic pressure and to obtain arterial blood samples. Left-sided thoracotomy was performed at the fifth intercostal space.

In three dogs, a 7F catheter with seven pores was placed at the brachiocephalic artery via the left femoral artery to inject contrast material. The external carotid artery was ligated proximally on both sides; the subclavian artery was also ligated bilaterally distal to the point at which the vertebral artery branches off. The contrast material injection was repeated during inhalation of CO_2 (2 L/min without altering oxygen supply or ventilation) and 60 minutes after completion of the CO_2 inhalation.

In the remaining three dogs, angiography was carried out by injecting contrast material via the vertebral artery while the brachiocephalic artery was partially occluded. After thoracotomy, a silicon tube bypass equipped with the flow-probe of an electromagnetic flowmeter (MFV2100, Nihon Kohden, Japan) was set between the left femoral artery and the left vertebral artery. An adequate amount of heparin was administered (13). Thirty seconds before the contrast material injection, the brachiocephalic artery was partially occluded. This procedure increased left vertebral flow to approximately twice the preoccluded value. Under this condition, contrast material was injected via the left vertebral artery. Without this procedure, the circle of Willis and its branches cannot be seen entirely via the vertebral artery.

In all dogs, contrast material with 30% nonionic iodine (iomeprol or iopamidol) was injected into the catheter (13 mL/s for 1 second) or the bypass (3 mL/s for 4 seconds) while the dogs were irradiated from the throat to the parietal direction in order to obtain a full image of the circle of Willis.

Image Analysis

The vessel diameter was measured semiautomatically on the digital image of a personal computer (Power Macintosh 8100/100AV, Apple Computer, Inc., Cupertino, CA) with ready-made freeware software (NIH image, version 1.60, National Institutes of Health, Bethesda, MD) with some modifications (details not shown). The image data stored in DAT were transmitted to the Macintosh via a local area network (Fig 1A). The method of diameter measurement was as follows: the transmitted image (1024 $\times$ 1024 pixels) was interpolated to the image with 2048 $\times$ 2048 pixels. A short temporary axis was delineated by hand at the vessel specified for measurement. The mean density profile perpendicular to the temporary axis was calculated (thin lines in insets in Fig 1B). To smooth the density profile, a running average with an appropriate window value (3 to 7 points) was obtained (thick lines in insets in Fig 1B). The vessel edges were defined as a pair of the two half-maximum points of the running averaged profile. The vessel diameter was calculated on the basis of the distance between the vessel edges. The pixel size was 9.77 $\times$ 9.77 μm, estimated from the visual field (20 mm/2048 pixels). Figure 1B shows an example of the diameter measurement; a pair of lines indicates the defined vessel edges. In the preliminary study, 37 vessel diameters were measured (52–667 μm) by two members of the research team working on this project (one a core member and the other a medical student). Linear regression analysis of the two measurements revealed a good linear correlation (r = .999, $Sy.x$ = 6.36) with a nearly ideal regression line (y = $1.017x-1.07$). The diameter of the reference copper wire (130 μm) was also measured at two points, and the values of 129.07 and 128.57 μm are shown in Figure 1B.

In several images, temporal subtraction was introduced to improve the image quality further. The subtracted images were created from the images obtained immediately before and during contrast material injection with custom-made image processing software at the workstation.

All numerical values obtained in the present study are expressed as means $\pm$ standard deviation (SD). We applied the

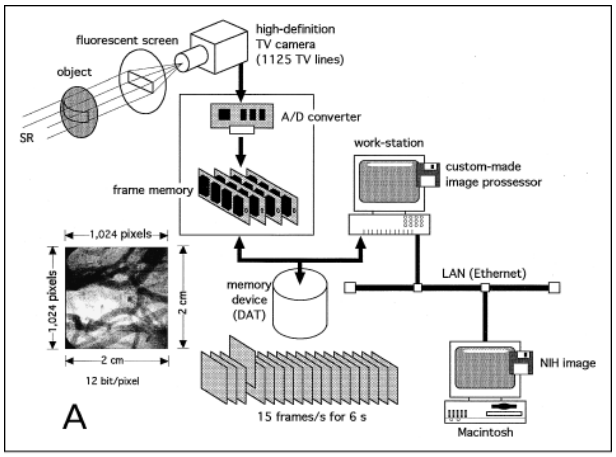

FIG 1. *A,* Schematic representation of the experimental set-up. DAT indicates digital audiotape; LAN, local area network; SR, synchrotron radiation.

B, An example of the method used to measure vessel diameters. Radiographic image shows cerebral vessels and a reference copper wire with a diameter of 130 μm (*arrowhead*). The mean density profiles (*thin lines*) and the running averaged mean density profiles (*thick lines*) for the two measured vessels (*a* and *b*) and the two sites of the reference wire (*c* and *d*) are shown. The diameter is calculated on the basis of the distance between the edges, which are defined as the two half-maximum points of the profile (see Methods). Ordinate represents density; abscissa, distance (μm). The measured value of the reference wire is approximately 130 μm. This angiogram was made from Figure 2.

unpaired *t*-test for comparison of the mean values of diameter and body weight between the two groups; that is, with and without partial occlusion of the brachiocephalic artery and an analysis of variance for repeated measures (ANOVA) to determine the significance of diameter, blood gas, and hemodynamic changes from baseline during and at completion of CO_2 inhalation. Differences were considered significant at $P < .05$.

Results

A representative angiogram obtained by injecting contrast material into the brachiocephalic artery is shown in Figure 2. The circle of Willis, the middle and posterior cerebral arteries, the anterior cerebellar artery, the basilar artery, and other small vessels were well seen. Two small branches arising from the communicating artery were visible on all the angiograms on either the right or the left side in all 26 images (see Fig 2). In one dog, one of these two branches arose directly from the proximal portion of the middle cerebral artery. In terms of canine anatomy, these two branches would presumably be the thalamoperforating artery or the anterior choroidal artery. On some images, the anterior cerebral artery, the internal ethmoidal artery, and the internal ophthalmic artery were also well seen. On occasion, some of these vessels were not visible because of the limited visual field size and incomplete filling of contrast material (laterality caused by selective injection, animal posture or both) but not because of inadequate sensitivity or spatial resolution in the present system. The visualization rates for the branches shown in Figure 3 ranged from 66% to 100%.

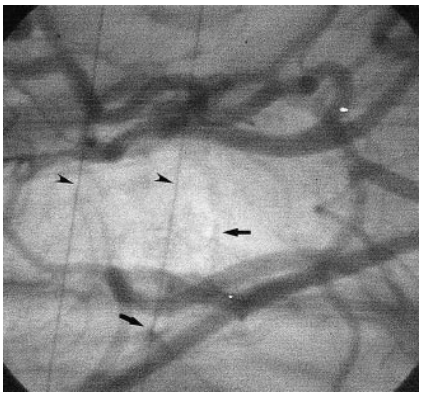

FIG 2. Cerebral angiogram obtained at baseline. The contrast material was injected into the brachiocephalic artery. *Arrows* indicate small branches of the circle of Willis; *arrowheads,* reference copper wires with a diameter of 130 μm. See Figure 4A for the names of the vessels. The field of view was 20 $\times$ 20 mm.

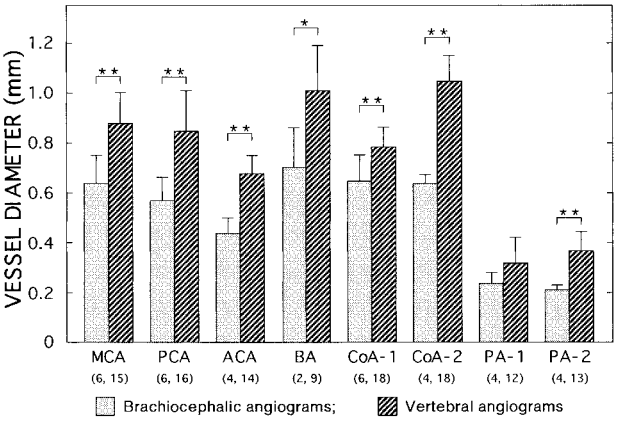

FIG 3. Vessel diameters, with and without brachiocephalic occlusion, were measured on brachiocephalic angiograms without occlusion (three images in three dogs) and vertebral angiograms with partial brachiocephalic occlusion (nine images in three dogs). The numbers of measured vessels on both sides are indicated in parentheses. The brachiocephalic angiogram of one representative dog is shown in Figure 2. MCA indicates middle cerebral artery; PCA, posterior cerebral artery; ACA, anterior cerebellar artery; BA, basilar artery; CoA-1, communicating artery between MCA and PCA; CoA-2, CoA between ACA and BA; PA-1 and PA-2 are the anterior and posterior vessels of the two small branches of the circle of Willis, respectively. Data are means $\pm$ SD. *$P = .053$, **$P < .001$ (unpaired *t*-test).

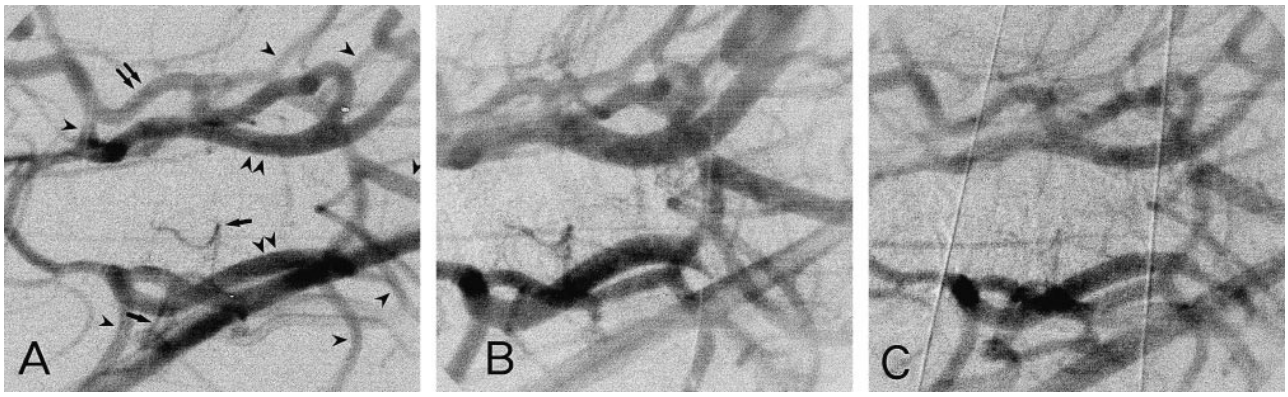

FIG 4. Temporal digital subtracted image of a cerebral angiogram obtained during CO_2 inhalation. The digital image obtained immediately before injection of contrast material into the brachiocephalic artery was subtracted from that obtained during the injection. The field of view was 20 × 20 mm.

A, Before CO_2 inhalation. The original image is the same as that shown in Figure 2. *Arrowheads* indicate large branches of the circle of Willis, namely, the middle cerebral artery, the posterior cerebral artery, the anterior cerebellar artery, and the basilar artery; *arrows,* small branches of the circle of Willis; *double arrowheads,* the internal carotid artery; *double arrows,* anastomotic ramus (between the internal carotid artery and the external ophthalmic artery). The anterior cerebellar artery arises from the communicating artery in the dog. $PaCO_2$ was 34.9 mm Hg.

B, During CO_2 inhalation, $PaCO_2$ was 125.5 mm Hg.

C, 60 minutes after the completion of CO_2 inhalation, $PaCO_2$ was 30.2 mm Hg.

The diameters of the cerebral arterial branches, including the small arteries, were measured on both vertebral angiograms with partial occlusion of the brachiocephalic artery (nine images in three dogs) and on brachiocephalic angiograms without occlusion (three images in three dogs) (Fig 3). The diameters of the large branches ranged from 400 to 1200 μm; those of the small branches, from 190 to 510 μm (PA-1 and PA-2 in Fig 3). We compared the diameters of these vessels on the brachiocephalic angiograms with those on the vertebral angiograms in order to examine the effects of brachiocephalic occlusion (Fig 3). The diameters were significantly larger in the latter than in the former. Body weights did not differ significantly between the two groups (10.1 ± 0.4 kg vs 9.2 ± 1.0 kg). These results suggest that partial occlusion of the brachiocephalic artery caused vasodilatation of both large and small arteries. Vertebral angiography without brachiocephalic occlusion revealed only spinal branches, the circle of Willis not being visible (data not shown).

The temporal digital subtraction technique improved angiographic quality by reducing the background. As an example, temporally subtracted images are shown in Figure 4. Figure 4A was created from Figure 2. The contrast of the angiographic image was increased and the vessels can be identified more clearly in Figure 4A than in the original images in Figure 2.

Brachiocephalic angiograms revealed that inhalation of CO_2 dilated both large and small arteries in all three dogs (Fig 4). These diameter changes are summarized in Figure 5, and blood gases and hemodynamic data in the Table. Representative subtracted images under CO_2 inhalation are shown in Figure 4B. In all of the measured arteries, significant vasodilatation was noted during CO_2 inhalation. Sixty minutes after completion of CO_2 inhalation, the diameters of the vessels had not been fully restored to their baseline values (Figs 4C and 5), although the levels of arterial blood gases decreased toward baseline (see Table).

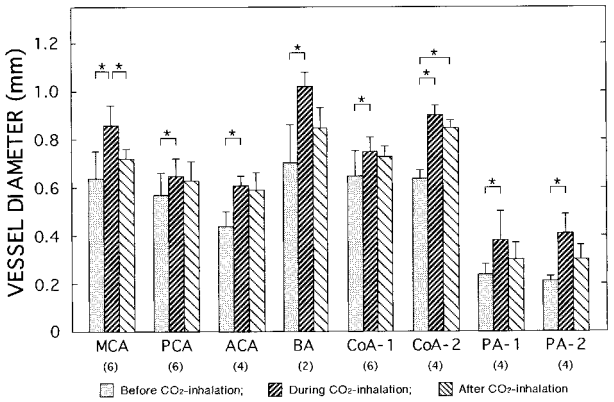

FIG 5. Effects of CO_2 inhalation on changes in vessel diameters in the brains. Vessel diameters were measured on brachiocephalic angiograms before CO_2 inhalation, during CO_2 inhalation (2 L/min), and 60 minutes after completion of CO_2 inhalation in three dogs. The numbers of vessels examined on both sides are indicated in parentheses. Images from one representative dog are shown in Figure 4. In one dog, the basilar artery was outside the field of view. Abbreviations are the same as in Figure 3. Data are means ± SD. *$P < .05$ (ANOVA).

Discussion

Using monochromatic synchrotron radiation, a high-definition TV camera, and digital image processing with the present angiographic system allowed us to visualize small vessels deep in the brain as well as to evaluate their diameters quantitatively. Monochromatic synchrotron radiation made it possible to detect even small amounts of

Blood gases and hemodynamic data during CO_2 inhalation in three dogs

	Before CO_2 Inhalation	During CO_2 Inhalation	60 Minutes after Completion of CO_2 Inhalation
PaO_2 (mm Hg, n = 3)	91.7 ± 4.0	120.3 ± 17.9	77.7 ± 14.6†
$PaCO_2$ (mm Hg, n = 3)	28.0 ± 6.7	101.5 ± 25.5*	28.7 ± 5.2†
pH (n = 3)	7.422 ± 0.074	6.949 ± 0.117*	7.297 ± 0.085†
Mean aortic pressure (mm Hg, n = 2)	123 ± 67	133 ± 53	113 ± 53
Heart rate (beats per minute, n = 2)	150 ± 71	145 ± 42	155 ± 14

Note.—Data are means ± SD. In one dog, hemodynamic data were not measured.

* $P < .05$ vs before CO_2 inhalation.

† $P < .05$ vs during CO_2 inhalation (ANOVA).

iodine and for the high-definition TV camera to delineate the images. The digital image processing enabled us to perform the diameter measurements with negligible interobserver differences and to improve the image quality. With the present system, the diameter of the smallest detected vessel was 60 μm (Fig 1B). We were able to visualize the small branches of the circle of Willis clearly and to measure their diameters (190 to 510 μm) on all angiograms with no significant interobserver differences. Our system has a pixel size of 9.77 × 9.77 μm and is capable of separating adjacent lead lines of 16 lp/mm on the X-ray modulate-transfer-function chart. Saeki and Rhoton (14) reported that the diameter of the human anterior choroidal artery is 0.5 to 2.3 mm. Generally, on conventional film-screen angiography, brain vessels with a diameter of less than 0.3 mm cannot be measured (5). Even with the use of a small X-ray focal spot (40 μm), brain vessels with a diameter of 0.2 mm still cannot be measured in rabbits and ferrets (15). Digital subtraction angiography with a 1024 matrix for clinical use has poorer spatial resolution than conventional film-screen angiography (16).

The present system also allowed quantitative evaluation of vascular diameter changes with vasodilating interventions. During CO_2 inhalation, significant vasodilatation was confirmed (Figs 4 and 5). Vasodilatation was also produced by partial occlusion of the brachiocephalic artery (Fig 3). Without brachiocephalic occlusion, contrast material injected into the left vertebral artery did not reach the circle of Willis.

Another advantage of the present system is that measurements of the vessels' diameters were performed semiautomatically by the computer (Fig 1B). When vessel diameters were measured manually using micrometers, calculations had to be made by an investigator without knowledge of the purpose of the measurements (17). Our system has little measurement bias, however, as indicated by the results of regression analysis of the measurements done by two members of the research team (see Methods). In addition, the digitized image acquisition system allowed transfer of the images to personal computers without loss of spatial resolution. On a personal computer, various types of software are applied for quantitation of vessel diameters.

The benefits of monochromatic synchrotron radiation and the high-definition TV camera have already been reported (6). Briefly, synchrotron radiation, which has an enormous number of photons, permits monochromatization at an energy level of 33.3 keV, enhancing sensitivity for the iodinated contrast material. The high-definition TV camera has high sensitivity and fine resolution.

Conclusion

The present angiographic system has monochromatic synchrotron radiation, a high-definition TV camera, and digital image processing that is useful not only for visualizing small vessels deep in the brain but also for quantitating their diameters; the present system makes possible direct, minimally invasive evaluation of vasodilatation and vasospasm in both large and small vessels. Visualization and quantitation of the small branches of the circle of Willis suggest that the present system may be useful for identification of the small vascular segments related to small cerebral infarctions and transient ischemic attacks in humans.

Acknowledgments

We thank Masami Ando and Osamu Shimomura (National Laboratory for High Energy Physics), Kenkichi Tanioka and Misao Kubota (NHK Science and Technical Research Laboratories), Hiroshi Kato (Eisai Co. Ltd.), and Tomoaki Miyazawa (Nihon Schering Co. Ltd.) for their valuable cooperation in this project and Yoshiro Iwata and Noriharu Yanagimachi for their useful comments.

References

1. Samuelsson M, Soderfeldt B, Olsson GB. **Functional outcome in patients with lacunar infarction.** *Stroke* 1996;27:842–846
2. Clavier I, Hommel M, Besson G, Noelle B, Perret JE. **Long-term prognosis of symptomatic lacunar infarcts: a hospital-based study.** *Stroke* 1994;25:2005–2009
3. Salgado AV, Ferro JM, Gouveia OA. **Long-term prognosis of first-ever lacunar strokes: a hospital-based study.** *Stroke* 1996; 27:661–666
4. Wardlaw JM, Lewis SC, Dennis MS, Counsell C, McDowall M. **Is visible infarction on computed tomography associated with an adverse prognosis in acute ischemic stroke?** *Stroke* 1998;29: 1315–1319

5. Takahashi M, Bussaka H, Nakagawa N. **Evaluation of the cerebral vasculature by intraarterial DSA–with emphasis on in vivo resolution.** *Neuroradiology* 1984;26:253–259
6. Mori H, Hyodo K, Tanaka E, et al. **Small vessel radiography in situ by using monochromatic synchrotron radiation.** *Radiology* 1996;201:173–177
7. Hyodo K, Nishimura K, Ando M. **Coronary angiography project at the photon factory using a large monochromatic beam.** In: Ebashi S, Koch M, Rubenstein E, eds. *Synchrotron Radiation Handbook.* Amsterdam: Elsevier Science; 1991:55–94
8. Mori H, Hyodo K, Tobita K, et al. **Visualization of penetrating transmural arteries in situ by monochromatic synchrotron radiation.** *Circulation* 1994;89:863–871
9. Tanioka K, Yamazaki J, Shidara K, et al. **Avalanche-mode amorphous selenium photoconductive target for camera tube.** *Adv Electronics Electron Phys* 1988;74:379–387
10. Umetani K, Kajiyama T, Ueda K, Takasaki Y, Yokouchi H. **High-sensitivity digital radiography using an avalanche-type image pickup tube camera.** *Proc SPIE* 1994;2163:361–365
11. Umetani K, Ueki H, Ueda K, et al. **High-spatial-resolution medical-imaging system using a HARPICON camera coupled with a fluorescent screen.** *J Synchrotron Radiat* 1996;3:136–144
12. Tanaka Y, Mori H, Tanaka E, et al. **Synchrotron radiation microangiography using an avalanche-type high-definition video camera.** In: Ando M, Uyama C, eds. *Medical Applications of Synchrotron Radiation.* Tokyo: Springer-Verlag; 1998:42–53
13. Chujo M, Mori H, Tanaka E, Nakazawa H, Okino H. **Inhibitory effects of nicorandil on sympathetic coronary vasoconstriction.** *Cardiovasc Res* 1994;28:917–922
14. Saeki N, Rhoton AJ. **Microsurgical anatomy of the upper basilar artery and the posterior circle of Willis.** *J Neurosurg* 1977; 46:563–578
15. Harder DR, Schulte ML, Clough AV, Dawson CA. **An angiographic method for in vivo study of arteries of the circle of Willis in small animals.** *Am J Physiol* 1992;263:H1616–H1622
16. Harrison MJ, Johnson BA, Gardner GM, Welling BG. **Preliminary results on the management of unruptured intracranial aneurysms with magnetic resonance angiography and computed tomographic angiography.** *Neurosurgery* 1997;40:947–955
17. Hino A, Weir BKA, Macdoonald RL, Thisted RA, Kim C-J, Johns LM. **Prospective, randomized, double-blind trial of BQ-123 and bosentan for prevention of vasospasm following subarachnoid hemorrhage in monkeys.** *J Neurosurg* 1995;83:503–509